# Robust Proportional ECMS Control (RPEC) of a Parallel Hybrid Electric Vehicle

Wisdom Enang [1*], Chris Bannister [1]

(1) University of Bath, Bath, UK
(*) Corresponding Author (wpe20@bath.ac.uk, wisdom_enang@yahoo.co.uk)

## ABSTRACT

Improved fuel efficiency in hybrid electric vehicles, requires a fine balance between internal combustion engine usage and battery energy, using a carefully designed energy management control algorithm.

Numerous energy management strategies for hybrid electric vehicles have been proposed in literature, with many of these centred on the Equivalent Consumption Minimization Strategy (ECMS) due to its potential for online implementation. The key challenge with the equivalent consumption minimisation strategy lies in estimating or adapting the equivalence factor in real time such that reasonable fuel savings are achieved without over-depleting the battery state of charge at the end of the defined driving cycle.

To address the challenge, this paper proposes a novel proportional state of charge feedback ECMS controller which simultaneously optimises and selects the adaption factors (proportional controller gain and initial equivalence factor) as single parameters which can be applied in real time, over any driving cycle. Unlike other existing state of charge feedback methods, this approach solves a conflicting multi-objective optimization control problem, thus ensuring that the obtained adaptation factors are optimized for robustness, charge sustenance and fuel reduction.

The potential of the proposed "Proportional ECMS controller" was thoroughly explored over a number of legislative and real-world drive cycles with varying vehicle power requirements. The results showed that, whilst achieving fuel savings in the range of 8.40 to 19.68% depending on the cycle, final battery state of charge could be optimally controlled to within ±5% of the target battery state of charge.

***Keywords:***

***Equivalent consumption minimisation strategy control, hybrid electric vehicles, Online control of hybrid electric vehicles, optimisation of hybrid electric vehicles, dynamic programming, optimal control of hybrid electric vehicles, control of hybrid electric vehicles, vehicle modelling, Parallel hybrid electric vehicles.***

## 1 INTRODUCTION

The gradual decline of global oil reserves, in addition to stringent emission regulations around the world, has made even more critical the need for improved vehicular fuel economy [1-3]. In recent years, the scientific community and industries alike have proposed a variety of innovations to face this challenge, coming up with new solutions in the aspect of hybrid powertrain architectures. Hybrid electric vehicles (HEVs) are able to address this problem by introducing a powertrain with an additional propulsion system, constituted in its simplest form by an electric energy storage unit (an electric battery), an electric torque actuator (an electric motor), and a device which couples together the electric driveline and the thermal driveline. The additional driveline allows for greater

flexibility in engine use while ensuring the fulfilment of the power request at the wheels.

In comparison to conventional vehicles, HEVs offer a number of advantages. The most popular of such advantages is the possibility of downsizing the original internal combustion engine while meeting the power demand at the wheels. This advantage is brought about by the capability of the hybrid powertrain to deliver power to the wheels from both the internal-combustion engine and the electric motor at the same time, thus resulting in reduced fuel consumption[4, 5].The introduction of an electric driveline in an HEV also allows for the regeneration of kinetic braking energy, which would otherwise be lost to mechanical brakes in conventional vehicles. Aside from fuel consumption related advantages, the use of HEVs also presents the possibility of cranking the engine with the electric motor, which allows for the removal of the starter motor from the powertrain. This new cranking procedure will allow for a faster, smoother and more improved cranking technique, as in the case of inertia cranking [6].

Crucial to achieving the aforementioned advantages is a real time control strategy capable of coordinating the on-board power sources in order to maximise fuel economy and reduce emissions. HEV power management strategies could be broadly classified into, optimisation-based methods which control the power split using exact knowledge of the future vehicle power demand and rule based real time implementable methods which control the power split without exact knowledge of the future vehicle power demand.

Rule-based methods are based on heuristics and engineering intuition which define how the powertrain should respond to each situation. Consequently, these strategies are easy to implement online but do not contain any explicit optimization [7]. Most-rule based HEV control methods are created with the goal in mind of reducing fuel consumption to the greatest degree. As such, the rules defining the strategy are usually directed at employing the engine at its high efficiency area, as well as exploiting regenerative braking as much as possible. The development of rule-based HEV control methods is generally articulated in two steps: the first being the definition of the relevant rules for the powertrain control, and the second being calibration of the strategy, which is typically carried out by means of simulations on a vehicle model. The main advantage of rule based HEV control methods lies in their simplicity, which makes them fairly easy to understand and implement on actual vehicles[8-14]. Owing to their low computational demand, natural adaptability to online-applications, good reliability and satisfactory fuel consumption results, rule-based control strategies have monopolised the production vehicle market. Despite their widespread utilisation, rule-based HEV control methods still present some significant challenges. Typically, in a rule-based HEV control strategy, a huge amount of time and investment in qualified workforce is required to develop the strategy, owing to the long process of rules definition and calibration process. This situation is further worsened by the fact that the rules need to be redefined for every new driving condition and powertrain, thus posing some questions about the robustness of rule based HEV control strategies [15]. In addition to this, recent research studies show that in comparison with optimisation methods, rule-based HEV control methods produce inferior but satisfactory fuel consumption results [16].

In comparison, optimisation-based control strategies decide the control signals either by minimising the sum of the objective function over time (global optimisation) or by instantaneously minimising the objective function (local optimisation). Global optimisation strategies solve the control problem as a whole along the entire driving cycle, thus having both an advantage and a drawback. The advantage is that these strategies yield the optimal solution to the control problem, thanks to prior knowledge of the driving cycle. The drawback is that such strategies cannot be implemented in real time, due to the need for prior knowledge of the entire driving cycle. Dynamic programming is often employed in HEV energy management problems as a global optimisation technique to find the absolute optimal control policy for a specific driving cycle, and it serves as a benchmark for other control strategies [17-23].These energy management problems could be single objective or

multi-objective as in the case of simultaneously optimising for fuel economy and emissions [24].

Conversely, local optimisation techniques reduce global optimisation problems into a succession of local optimisation problems. This eliminates the need for future driving information, thus making it possible for the strategy to be implemented in real time. Despite yielding marginally suboptimal results in comparison to global optimisation strategies, local optimisation strategies have received the greatest research attention in HEV control. The Equivalent Consumption Minimisation Strategy (ECMS) [25-29] and Pontryagin's minimum principle (PMP) [30, 31]feature as the most popular of these techniques among researchers. PMP is based on the instantaneous minimisation of a Hamiltonian function over a driving cycle [32, 33]. Kim *et al.*[32] employed PMP to solve an energy management problem for a power-split HEV architecture. In that study, the authors showed that by setting a correct initial estimate of the co-state, instantaneous minimisation of the Hamiltonian function over a driving cycle yields a control policy that closely matches results from dynamic programming when the state boundary conditions are met. Considering that PMP is a shooting method that solves a boundary value problem, the resulting control strategy is non-causal and thus not implementable online.

A more readily implementable local optimisation approach is the ECMS [25, 33, 34]. ECMS was first developed based on the heuristic concept that the energy used to drive a vehicle over a driving cycle ultimately comes from the engine, and as such the hybrid system merely serves as an energy buffer [25]. This strategy is based on the instantaneous minimisation of a cost index, which is the sum of a number of operation metrics weighted by equivalence factors. Variations to ECMS optimization control strategy have been reported by a number of studies. Examples of these variations include the Adaptive ECMS [34-36] and Telemetry ECMS [37], which adjust the equivalence factor based on past driving data and a prediction for the future. Although widely reported as successful, these adaptive techniques can suffer from several drawbacks which currently impede their popularity among commercial HEVs. For example, telemetry ECMS requires additional predictive hardware, such as a Global Positioning System (GPS) , to be integrated within the vehicle which comes at an additional cost. Similarly, the adaptive ECMS is subject to additional computational burden and uncertainties. These uncertainties can be caused by a limited number of representative driving cycles (to account for different driving conditions), the impacts of driving pattern recognition on the controller performance, the impact of window size on pattern recognition and a limited number of "cycle characterizing" quantities. Mitigating these issues involves the development of an equivalence factor adaptation technique based on single adaptation parameters (proportional controller gain and initial equivalence factor) which can be applied in real time over any driving cycle. Using this technique, battery state of charge deviations of up to 20% between the beginning and the end of driving cycles have been reported in literature [38]. In view of this challenge, a novel, simple, but effective robust proportional ECMS controller is proposed and tuned over seven standard driving cycles, to ensure that real time fuel savings are achieved whilst keeping the deviation between the initial and final battery state of charge within $\pm$5%.

The disposition of this paper is outlined as follows: First, the energy management problem for a parallel HEV is quantified and defined, after which a quick derivation of the ECMS strategy is carried out using the Pontryagin's Minimum Principle. Next, a brief overview about the challenges currently facing the commercialisation of ECMS strategies is discussed alongside the different solutions which have been proposed by different studies in literature. Afterwards, the proportional ECMS control strategy is developed, tuned and simulated over some standard driving cycles in real time. Finally, simulation results from the proportional ECMS controller are compared to results obtained from other ECMS controllers published in literature.

## 2 THE ENERGY MANAGEMENT PROBLEM

Accurate vehicle modelling is imperative for the development of a robust energy controller. A quasi-static modelling approach is employed to mathematically represent the dynamics of a parallel HEV. Detailed modelling and validation of this vehicle was carried out in a previous study [39] and, therefore, is not covered in this paper. This study, however, builds on the already modelled vehicle (whose data is detailed in Appendix 1) to define and solve the optimal HEV energy management problem in real time. The layout of the vehicle architecture is provided in Figure 1 for illustrative purposes.

The rest of this section references formulas which were derived in a previous study by Enang *et al.*[39].

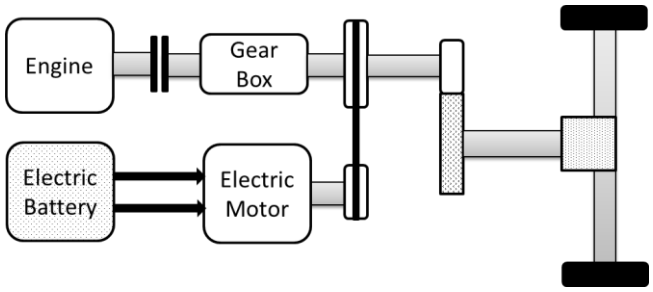


Figure 1: Parallel hybrid electric vehicle [39]

The optimal control problem in an HEV consists of finding the sequence of controls $U(t)$ that leads to the minimisation of the performance index $J$, defined as:

$$J\left(X(t_0), U(t), X(t_f)\right) = \emptyset\left(X(t_0), X(t_f)\right) + \sum_{t_0}^{t_f} L(X(t), U(t), t)dt \quad (1)$$

Where $t$ represents the time, $U(t)$ is the control action, $X(t)$ is the state variable, $[t_0, t_f]$ is the optimisation horizon, $L$ is the instantaneous cost function and $\emptyset$ is the terminal cost (i.e. cost due to the final value of the state), which physically translates to the fuel lost or gained in order to attain charge sustenance. In the absence of plug in charging facilities on parallel HEVs, enforcing a charge sustaining constraint at the end of the driving cycle ensures that the hybrid system is readily available for use at any time and that the durability of the battery (battery life) is increased via reduced depth of discharge (DOD). Battery life directly depends on the total energy throughput that its active chemicals can tolerate. Ignoring other ageing effects, the total energy throughput is fixed, such that 1 cycle of 100% DOD is roughly equivalent to 2 cycles at 50% DOD, 10 cycles at 10% DOD and 100 cycles at 1% DOD.

In this energy management problem, the optimal control law is denoted by $U^*(t)$, and the corresponding optimal state trajectory is denoted by$X^*(t)$. By definition, the optimal control is such that:

$$J\left(X(t_0), U^*(t), X^*(t_f)\right) \leq J\left(X(t_0), U(t), X(t_f)\right) \quad (2)$$

The state variable $X(t)$ in this energy management problem is the battery state of charge (SOC), which is a measure of the charge left in a battery as a proportion of the total battery capacity. In simulation, the battery SOC is calculated as an integral of battery current over the maximum possible battery charge. The control vector $U(t)$ in this energy management problem is the electric motor mechanical power $P_{motor}$ and the instantaneous cost $L$ is the vehicular fuel consumption $\dot{m}_f$.

Considering the convex nature of the internal-combustion engine model, fuel consumption could be expressed as a function of engine speed and torque $\dot{m}_{f\ engine}(W_{ICE}, T_{ICE})$ (Figure 2).Using the longitudinal model of a parallel HEV [39] as expressed by:

$$T_{ICE} = \frac{(m\frac{dV_v}{dt} + \sum(F_{aero} + F_{rolling} + F_{grade} + F_{extra}))R_w}{FDR\ G_E\ Eff} - \frac{P_{motor}}{G_E\ FDR\ W_{wheel}\frac{2\pi}{60}} \quad (3)$$

$$W_{ICE} = W_{wheel}\ FDR\ G_E\frac{2\pi}{60} \quad (4)$$

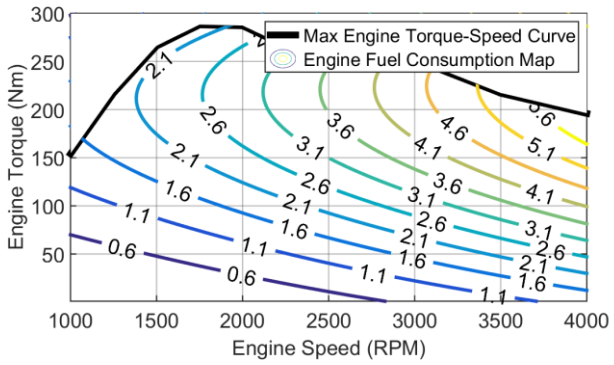


Figure 2: Engine fuel consumption map[39]

The instantaneous cost (fuel consumption) could be expressed as a function of the control action thus: $\dot{m}_{f\ engine}(P_{motor})$.

Equation 5[39] is defined to measure the effect of each control policy on the battery state of charge.

$$SOC_{t+1} = SOC_t \pm \frac{V_{oc} - \sqrt{{V_{oc}}^2 - 4RP_{motor}\eta_{motor}\,\eta_{batt}}}{2RQ} \quad 5$$

Where:-

$\eta_{batt} = \eta_{gen} \times \eta_{chg}$ Charge: (+)

$\eta_{batt} = \frac{1}{\eta_{dis}}$ Discharge: (-)

$\eta_{gen} = 0.4$

*(Assumed low to account for loses during regenerative energy conversion)*

$\eta_{dis} = \eta_{chg} = 80\%$ (Typical of lithium ion batteries, which is the same battery used in this study (see Appendix 1)).

Where: $\frac{V_{oc} - \sqrt{{V_{oc}}^2 - 4RP_{motor}\eta_{motor}\,\eta_{batt}}}{2RQ}$ is a measure of the current flowing through the battery. Consequently, the evolution of the battery state of charge as a function of the battery current could be expressed thus:

$$\dot{SOC}_t = -\frac{I_t}{Q} \quad 6$$

Limitations in the operating range of the electric motor and the battery mean that constraints must be applied to the state (battery state of charge and control policies (electric motor mechanical power $P_{motor}$) (as shown in Table 1) in order to ensure that both the electric motor and battery operate within their safe bounds.

| | |
|---|---|
| *Initial state constraint* | $SOC_{t_0} = 60$ |
| *Charge sustainability state constraint* | $SOC_{t_f} = SOC_{t_0} = 60$ |
| *Instantaneous state constraint* | $SOC_{min} \leq SOC \leq SOC_{max}$ |
| *Instantaneous control constraint* | $P_{motor} \leq P_{motor_{max}}(W_{motor})$ |

Table 1: Energy management control and state constraints

## 3 ECMS DERIVATION FOR ENERGY MANAGEMENT

The ECMS is based on the engineering intuition that in a charge sustaining HEV, the energy used to propel the vehicle originates from the fuel, and the battery is only used as an energy buffer. The ECMS, originally derived as a real time realisation of PMP, mathematically reformulates a global optimisation problem into a local optimisation problem, where the equivalent fuel consumed is minimised at each instant.

PMP, originally proposed by the Russian mathematician Lev Pontryagin in 1958[40], provides a set of conditions necessary to ensure the optimisation of the control policy. PMP is a special case of the Euler-Lagrange equation of variational calculus, whose principle lies in the definition of the Hamiltonian function of the system.

In a charge sustaining HEV application, the principle is applied using the following steps:

**Step 1**

The Hamiltonian function or cost function to be minimised is defined thus as shown in Equation7.

$$H(SOC_t, P_{motor}, \gamma_t, t) = \dot{m}_{f\ engine}(P_{motor}) + \gamma_t S\dot{O}C_t \quad (7)$$

The Hamiltonian function defined in Equation 7 represents the instantaneous form of the integral optimisation cost function introduced in Equation 1.

**Step 2**

For optimality to be ensured, the control inputs $P_{motor}$ are chosen such that the Hamiltonian condition

$$H({SOC_t}^*, {P_{motor}}^*, {\gamma_t}^*, t) \leq H(SOC_t, P_{motor}, \gamma_t, t) \quad (8)$$

is satisfied and the Hamiltonian is minimised, subject to the constraints listed in Table 1.

**Step 3**

The state and co-state equations are solved thus:

*State equation:* $S\dot{O}C_t = -\left(\frac{I_t}{Q}\right) = \left(\frac{dH}{d\gamma_t}\right)$ where $I_t$ (A) is the current flowing through the battery and $Q(Ah)$ is the maximum possible battery charge.

*The co-state equation:* $\dot{\gamma}_t = -\left(\frac{dH}{dSOC_t}\right)$

If the Hamiltonian function in Equation (7) is combined with the system state equation, we obtain Equation 9 as detailed below.

$$H(SOC_t, P_{motor}, \gamma_t, t) = \dot{m}_{f\ engine}(P_{motor}) - \gamma_t \frac{I_t}{Q} \quad (9)$$

When $I_t = \frac{\eta_{motor} \times P_{motor}}{V_{batt}}$ is substituted in Equation (9), the Hamiltonian function can be re-expressed thus as shown below:

$$H(SOC_t, P_{motor}, \gamma_t, t) = \dot{m}_{f\ engine}(P_{motor}) - \gamma_t \frac{\eta_{motor} \times LHV \times P_{motor}}{Q \times LHV \times V_{batt}} \quad (10)$$

*Where $\eta_{motor}$is the motor efficiency, $LHV$ is the lower heating value ofthe fuel, $V_{batt}$ is the battery voltage and $\gamma_t$ is the co-state of the controller.*

Under the definition of equivalence factor thus:

$$\varepsilon_t = \frac{LHV \times \gamma_t}{Q \times V_{batt}} \quad (11)$$

Where - $\infty < \gamma_t < 0$, the Hamiltonian function can be expressed as:

$$H(SOC_t, P_{motor}, \gamma_t, t) = \dot{m}_{f\ eq}(SOC_t, P_{motor}, \gamma_t, t) = \dot{m}_{f\ engine}(P_{motor}) + \varepsilon_t \frac{\eta_{motor} \times P_{motor}}{LHV} \quad (12)$$

*Where $\dot{m}_{f\ eq}(SOC_t, P_{motor}, \gamma_t, t)$ is the equivalent fuel consumed by the vehicle.*

Under the assumption that the effect of the battery SOC on the equivalence factor is negligible[32], equation (12) can be expressed thus:

$$\dot{m}_{f\ eq}(SOC_t, P_{motor}, \gamma_t, t) = \dot{m}_{f\ engine}(P_{motor}) + \varepsilon \frac{\eta_{motor} \times P_{motor}}{LHV} \quad (13)$$

Where: $0 < \varepsilon < \infty$

| | |
|---|---|
| $\dot{m}_{f\ eq}(SOC_t, P_{motor}, \gamma_t, t)\ is$: | Equivalent fuel cost (g/s) |
| $\dot{m}_{f\ engine}(P_{motor})\ is$: | Engine fuel cost (g/s) |
| $\varepsilon \frac{\eta_{motor} \times P_{motor}}{LHV}\ is$: | Battery fuel cost (g/s) |

Physically, the equivalence factor $\varepsilon$ can be explained as the equivalent conversion ratio between the thermal energy from fuel and electrical energy.

As could be inferred from Figure 3, a low equivalence factor implies that electrical energy is cheaper than using fuel and therefore the controller encourages battery use. Conversely, a high equivalence factor implies that using electrical energy is expensive and therefore the controller reduces battery use.

Pictorially, the equivalent fuel cost function expressed in Equation (13) is shown in Figure 4. The lenticular nature of the equivalent fuel cost function means that the optimal solution is unique at each time instant.

Equation (13) is the mathematical representation of ECMS which will be applied in the rest of this study for the development of the robust real time HEV control strategy.

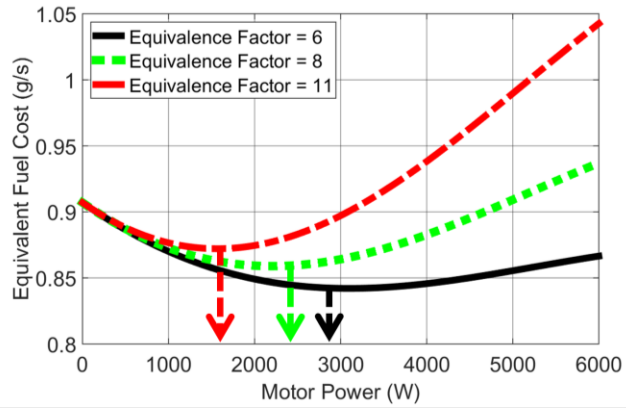


Figure 3: Impact of equivalence factor on optimal control input

*Power Demand = 40000 W, Motor Speed = 2000 RPM*

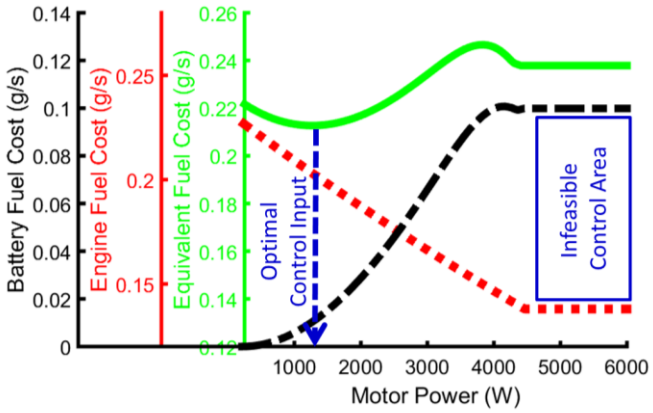


Figure 4: Impact of motor power on battery, engine and equivalent fuel cost. Power Demand = 20000 W, Equivalence Factor = 6, Motor Speed = 1000 RPM

## 4 DRIVING CYCLES

Understanding real world driving conditions in the form of driving cycles is instrumental to the design of an online robust optimal control strategy. There are 11 standard driving cycles (listed in Table 2) employed in this study as representatives of different driving scenarios.

| Driving cycle type | Total distance (m) | Total time (s) | Average positive acceleration ($m/s^2$) | Average driving speed (Km/h) |
|---|---|---|---|---|
| **NEDC** | 11017 | 1180 | 0.53 | 42.24 |
| **FTP72** | 11997 | 1369 | 0.43 | 36.60 |
| **JAPAN1015** | 4165 | 660 | 0.37 | 30.73 |
| **SC03** | 5766 | 596 | 0.42 | 40.38 |
| **NYCC** | 1903 | 598 | 0.47 | 16.63 |
| **HWFET** | 16503 | 765 | 0.16 | 77.76 |
| **IM240** | 3154 | 240 | 0.36 | 47.51 |
| **US06** | 12894 | 596 | 0.54 | 79.62 |
| **LA92** | 15802 | 1435 | 0.50 | 45.22 |
| **ARTEMIS U130** | 28737 | 1068 | 0.27 | 97.60 |
| **WLTC 3** | 23260 | 1800 | 0.41 | 46.30 |

Table 2: Standard driving cycle characteristics[41]

In order to emphasise the peculiarity of each selected driving cycle to this study, a novel two class grouping system is proposed as shown in Table 4. Using the proposed grouping system, the standard driving cycles used in this study are classified on the basis of aggressivity (quantified as the aggressivity factor (AGF)) and road type. The road type classification is based on the speed class grouping system originally proposed by Irene Berry [42], while the aggressivity classification is inferred from the AGF calculated in Table 3

for non-modal driving cycles (NYCC, FTP-72, SC03, IM240, WLTC 3, LA92, ARTEMIS U130, US06 and HWFET driving cycles) as the product of average positive acceleration and average driving speed, or for modal driving cycles (NEDC and JAPAN 1015 driving cycles) as the product of average driving speed and the square of average positive acceleration.

| Driving cycle type | Average positive acceleration ($m/s^2$) | Average driving speed (Km/h) | Aggressivity factor ($m^2/s^3$) |
|---|---|---|---|
| **NEDC** | 0.53 | 42.24 | 3.27 |
| **FTP72** | 0.43 | 36.60 | 4.36 |
| **JAPAN1015** | 0.37 | 30.73 | 3.16 |
| **SC03** | 0.42 | 40.38 | 4.76 |
| **NYCC** | 0.47 | 16.63 | 2.15 |
| **HWFET** | 0.16 | 77.76 | 3.39 |
| **IM240** | 0.36 | 47.51 | 4.75 |
| **US06** | 0.54 | 79.62 | 11.97 |
| **LA92** | 0.50 | 45.22 | 6.31 |
| **ARTEMIS U130** | 0.27 | 97.60 | 7.40 |
| **WLTC 3** | 0.41 | 46.30 | 5.27 |

Table 3: Standard driving cycle aggressivity factors

| | | Aggressivity Classification | | |
|---|---|---|---|---|
| | | **Calm (AGF < $4m^2/s^3$)** | **Moderate ($4 \leq$ AGF $\leq 6m^2/s^3$)** | **Aggressive (AGF > $6m^2/s^3$)** |
| **Driving type based on road type** | **Neighborhood driving (Average driving speed < 32Km/h)** | JAPAN1015, NYCC | | |
| | **Urban driving (32Km/h < Average driving speed < 72Km/h)** | NEDC | FTP72, SC03, IM240, WLTC 3 | LA92, ARTERMIS U130 |
| | **Highway driving (Average driving speed > 72Km/h)** | HWFET | | US06 |

Table 4: Standard driving cycle classification based on road type and aggressivity

Based on the proposed classification system, the NEDC driving cycle, for example, represents a calm urban driving scenario, while the LA92 and ARTERMIS U130 driving cycles are representatives of aggressive urban driving scenarios. The same interpretation applies to the rest of the driving cycles classified above.

# 5 ECMS SOLUTION TO ENERGY MANAGEMENT PROBLEM

## 5.1 Impact of equivalence factor on system dynamics

According to a number of studies [2, 25, 33, 35], there is a direct link between the equivalence factor and the battery state of charge usage over any driving cycle. The effect of this calibration is further shown in Figure 5 over the NEDC, FTP72 and HWFET driving cycles. From these plots, three main observations are apparent. Firstly, a single but cycle-specific optimal equivalence factor is found to be responsible for charge sustenance (final battery SOC = 60%) over each driving cycle. Secondly, the ECMS control strategy in its present form is highly inflexible. Consequently, a slight deviation in the estimation of the optimal equivalence factor would yield an undesired controller performance which is non-charge sustaining in real time. Finally, the equivalence factor is found to correlate inversely with cumulative fuel savings and proportionately with the final battery state of charge. The peculiar nature of each equivalence factor, as shown in Table 5, means that prior knowledge of the driving cycle is needed for the ECMS to produce charge-sustaining control policies, thus yielding an inherently offline control strategy.

Therefore, in order for ECMS to be employed online, the equivalence factor needs to be determined in an alternative way such that it does not rely on prior driving cycle information.

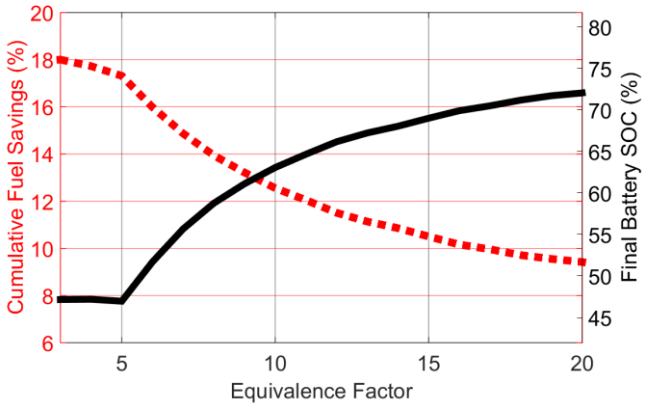


(a) NEDC driving cycle

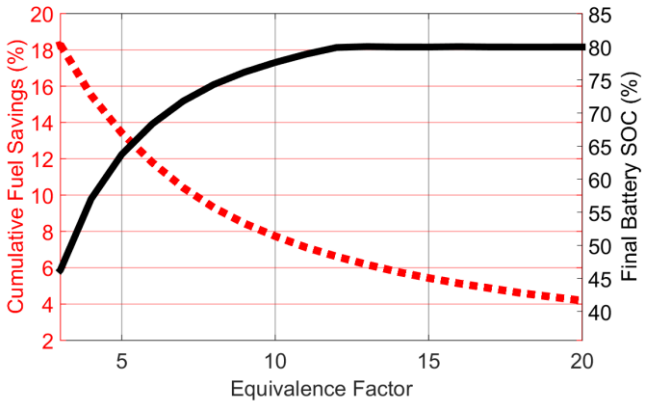


(b) FTP72 driving cycle

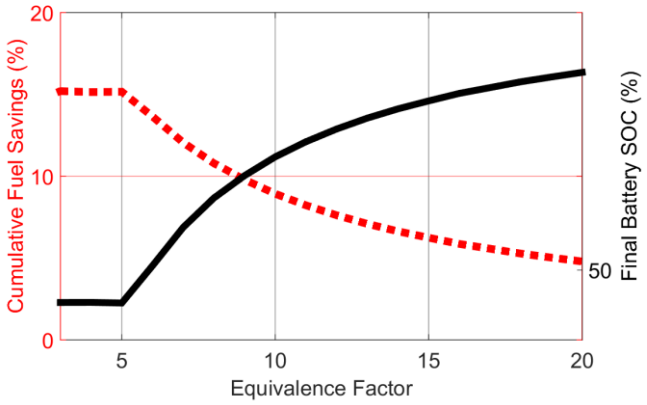


(c) HWFET driving cycle

Figure 5: Impact of equivalence factor on cumulative fuel savings and final battery state of charge

| Driving cycle | Equivalence factor | Final battery SOC (%) | Cumulative fuel savings (%) |
|---|---|---|---|
| **NEDC** | 8.512 | 60.00 | 13.57 |
| **FTP72** | 4.515 | 60.00 | 14.47 |
| **HWFET** | 8.050 | 60.00 | 10.76 |

Table 5: Equivalence factor and controller result for NEDC, FTP72 and HWFET driving cycle under charge sustenance

## 5.2 Existing equivalence factor adaptation strategies

Several techniques aimed at appropriately estimating or adapting the equivalence factor towards simultaneously achieving fuel savings and charge sustenance over different driving cycles in real time have been proposed since the introduction of the ECMS strategy. The first simplistic approach was setting the equivalence factor equal to one at all times and for any driving cycle [43]. This strategy was found to yield undesired controller results which were either charge depleting or charge hoarding, depending on the driving cycle in question. Consequently, strategies for adapting the equivalence factor online were created. Among some relevant examples are equivalence factor adaptation based on driving cycle prediction using GPS[37], driving pattern recognition [44] and battery SOC feedback[45]. In the equivalence factor adaptation method using driving cycle prediction, future driving conditions over a discrete prediction horizon are estimated using a GPS or intelligent transportation system (ITS) device and are used to adapt the equivalence factor accordingly online. In the equivalence factor adaptation method using driving pattern recognition, driving pattern recognition techniques are used online over discrete prediction windows to obtain an estimate of the optimal equivalence factors (pre-computed using offline optimisation) in different driving conditions. In the equivalence factor adaptation method using battery SOC feedback, the equivalence factor is dynamically adjusted in order to contrast the SOC variation, thus maintaining its value around the reference SOC value

(60%), which is considered to be constant. In comparison to the other existing methods, equivalence factor adaptation based on SOC feedback appears to be the most promising, viable and cost-effective method of realising a charge sustaining ECMS optimal control in real-time, as shown in Table 6. However, this potential is currently offset by its lack of flexibility (non-adaptability to varying driving conditions), which is the main inspiration for this research.

| Comparison Factors | Equivalence Factor Adaptation Based on Driving Cycle Prediction | Equivalence Factor Adaptation Based on Driving Pattern Recognition | Equivalence Factor Adaptation Based on SOC feed back |
|---|---|---|---|
| Computational load and cost | High | High | Low |
| Susceptibility to estimation errors | High | High | Low |
| Need for external prediction equipment | High | None | None |
| Real time implementation cost | High | Average | Low |
| Adaptability to varying driving conditions | High | High | Low |

Desired factors Undesired factors

Table 6: Comparison of different equivalence factor adaptation techniques

## 5.3 Proposed equivalence factor adaptation strategy

In view of the highlighted research gap with regards to equivalent factor adaption, the use of a simple proportional controller was proposed as shown in Figure 6. This adaption strategy ensures charge sustainability by adapting online the equivalence factor, thus impacting the relative convenience of thermal and electric operation. When the battery SOC value is higher than the reference SOC value (60%), the proportional controller dynamically adapts the equivalence factor such that electrical energy is deemed cheap and therefore battery use is increased. The reverse happens when the battery SOC value falls below the reference SOC value.

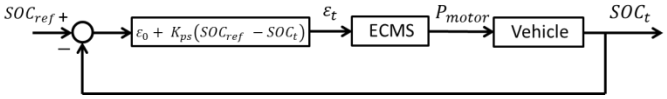


Figure 6: Equivalence factor adaptation based on a simple proportional controller

*Where: $\varepsilon_0$ is the initial value of the equivalence factor, $K_{ps}$ is the proportional controller gain and $SOC_{ref}$ (Charge sustaining SOC) is 60%.*

The proposed adaptation strategy differs conceptually from other existing SOC feedback adaptation techniques in the sense that while existing methods propose the selection of the proportional controller gain $K_{ps}$alone, thus making the controller performance heavily dependent on the intuitive estimate of the initial equivalence factor $\varepsilon_0$, this method simultaneously optimises and selects the proportional controller gain and initial equivalence factor as single parameters which can be applied in real time over any driving cycle. Unlike other existing SOC feedback methods, this approach solves a conflicting multi-objective optimisation control problem, thus ensuring that the obtained adaptation factors ($K_{ps}$, $\varepsilon_0$) are optimised for robustness, charge sustenance and fuel reduction.

In order to estimate an appropriate value for the initial equivalence factor $\varepsilon_0$ and theproportional controller gain $K_{ps}$ for this controller, a sensitivity analysis of its impact on cumulative fuel savings and final battery state of charge was carried out over the NEDC, FTP-72 and HWFET driving cycles as shown in Figure 7, Figure 8 and Figure 9.

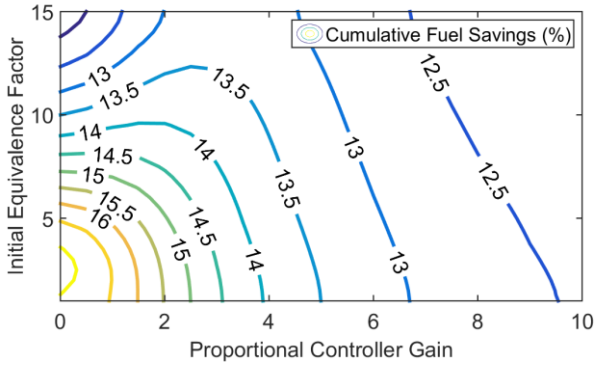


(a) Impact of initial equivalence factor and proportional controller gain on cumulative fuel savings

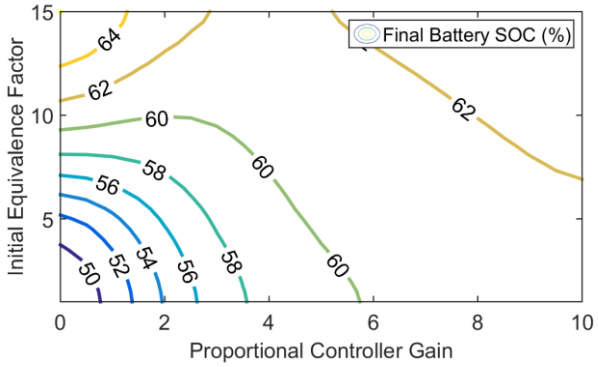


(b) Impact of initial equivalence factor and proportional controller gain on final battery SOC

Figure 7: Sensitivity analysis of initial equivalence factor and proportional controller gain over the NEDC driving cycle

From these figures, the following two key observations were made:

1. For all driving cycles analysed, an increase in proportional controller gain is found to correspond to an increase in controller robustness for SOC control, as well as a reduction in cumulative fuel savings (%) achieved.
2. As the proportional controller gain is increased, a significant change in gradient of the final battery SOC (%) curve is observed, thus resulting in a robust controller performance in which a change in initial equivalence factor has very little effect on the change in the final battery state of charge.

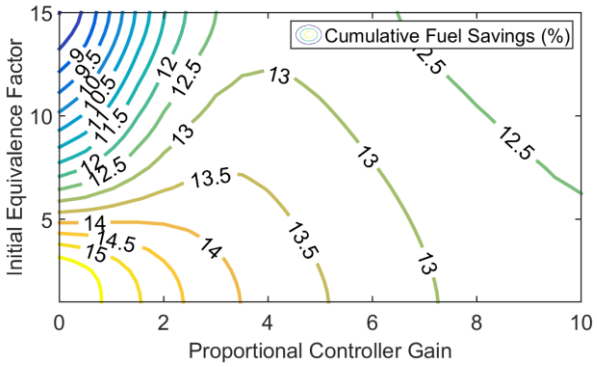


(a) Impact of initial equivalence factor and proportional controller gain on cumulative fuel savings

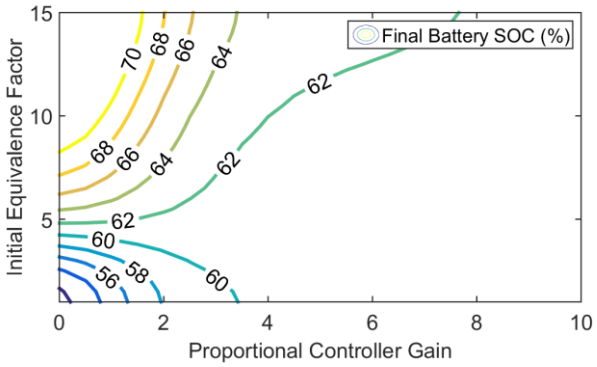


(b) Impact of initial equivalence factor and proportional controller gain on final battery SOC

Figure 8: Sensitivity analysis of initial equivalence factor and proportional controller gain over the FTP72 driving cycle

For each driving cycle, there exist a set of unique initial equivalence factors and proportional controller gains which yield a charge-sustainingperformance. Considering the fuel saving potential posed by each set of cycle specific controller adaptation factors, the control dilemma lies in simultaneously selecting an appropriate single initial equivalence factor and proportional controller gain which is optimised for fuel reduction, charge sustenance and robustness.

In order to select the appropriate value of initial equivalence factor and proportional controller gain for use in real-time optimal control of the HEV, the following unique steps were taken:

1. A sensitivity analysis was carried out, outlining the impact of initial equivalence factor and proportional controller gain on cumulative fuel savings and final battery state of charge over the NEDC, FTP-72, JAPAN 1015, NYCC, SC03, HWFET and IM240 driving cycle.

2. For each controller gain and equivalence factor, average the corresponding cumulative fuel savings (%) and final battery SOC (%) accordingly as shown in Figure 10.

3. For each set of average charge sustaining initial equivalence factor and controller gain, the corresponding average cumulative fuel savings (%) are plotted as shown in Figure 11.

4. The charge-sustaining adaptation parameter set (initial equivalence factor and proportional controller gain) with the highest average cumulative fuel savings (%) is selected and applied to the ECMS controller in real time (Figure 11).

5. Based on the steps listed above, an initial equivalence factor of 3.47 and a controller gain of 1.725 were selected for the real-time control of the modelled vehicle.

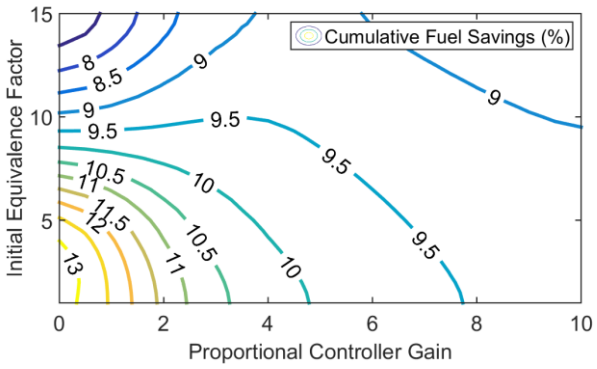


(a) Impact of initial equivalence factor and proportional controller gain on cumulative fuel savings

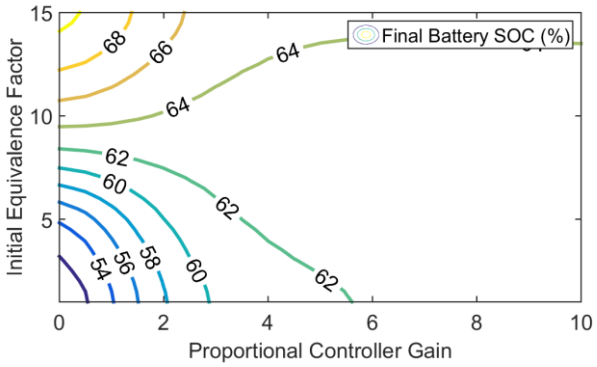


(b) Impact of initial equivalence factor and proportional controller gain on final battery SOC

Figure 9: Sensitivity analysis of initial equivalence factor and proportional controller gain over the HWFET driving cycle

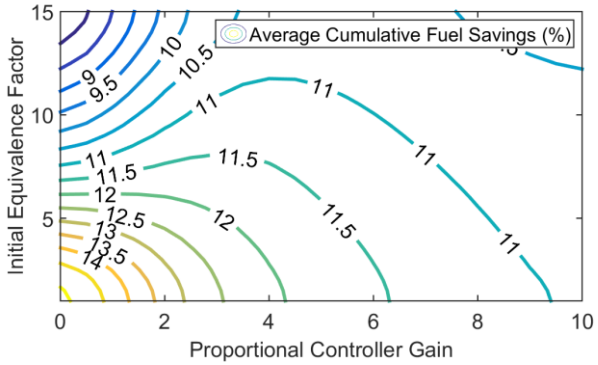


(a) Impact of initial equivalence factor and proportional controller gain on cumulative fuel savings

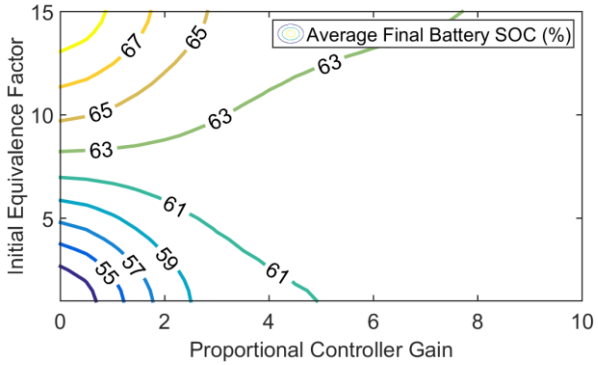


(b) Impact of initial equivalence factor and proportional controller gain on final battery SOC

Figure 10: Sensitivity analysis of initial equivalence factor and proportional controller gain: Averaged over NEDC, FTP72, JAPAN1015, NYCC, SC03, HWFET and IM240 driving cycle

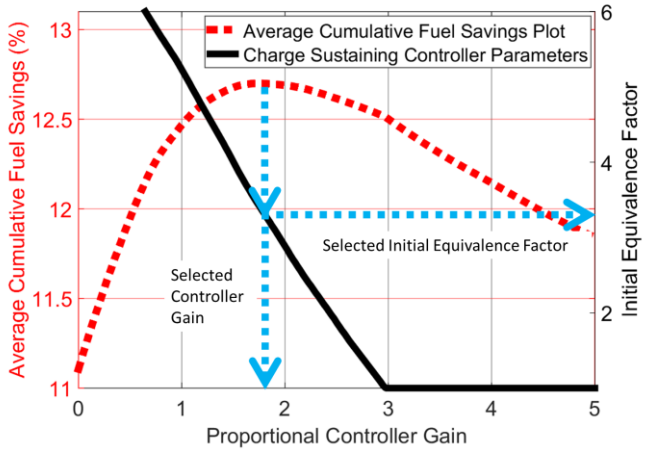


Figure 11: Selection of initial equivalence factor and proportional controller gain for real time HEV control

## 5.4 Real-time evaluation of the proposed proportional ECMS controller

### 5.4.1 Evaluation over standard driving cycles

In this section, the hybridisation potentials of the proposed "Robust Proportional ECMS Control" strategy (RPEC) are assessed over the US06, LA92, ARTEMIS U130 and WLTC 3 driving cycles in real-time on a vehicle simulation. In order to assess these potentials, the pre-estimated values of the initial equivalence factor (3.47) and the proportional controller gain (1.725) which was estimated in section 5.3 are applied.

Over the US06 driving cycle (Figure 12a),which represents an aggressive highway driving scenario in the US (see Table 4), the proposed controller is found to be charge depleting by 1.57% as shown in(Figure 12d), with a cumulative fuel savings of 8.40% as shown in (Figure 12c).

Unlike the US06 driving cycle, the LA92 driving cycle (Figure 13a) represents an aggressive urban driving scenario which typically offers more braking opportunities. Over this driving cycle, the motor was found to significantly participate in the vehicle braking, which is believed to be the prime contributor to the near-charge-sustaining performance of 60.61% (Figure 13d) achieved by the controller. In addition, a cumulative fuel savings of 10.40% was achieved over this driving cycle as shown in Figure 13c.

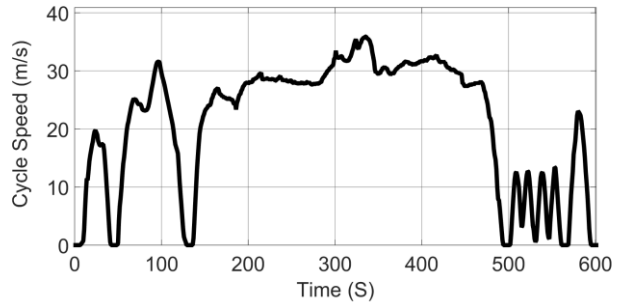


(a) US06 driving cycle profile

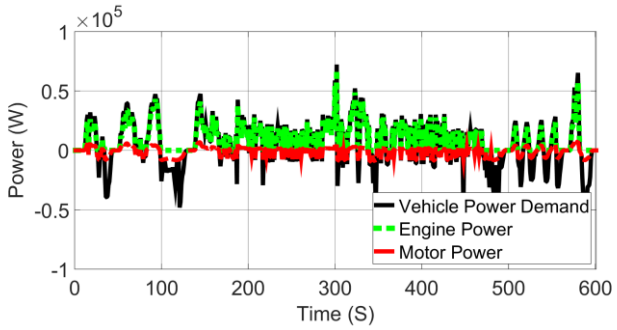


(b) Power split between electric motor and engine

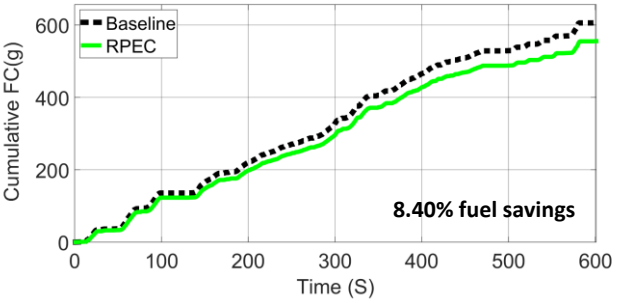


(c) Cumulative fuel consumption profile

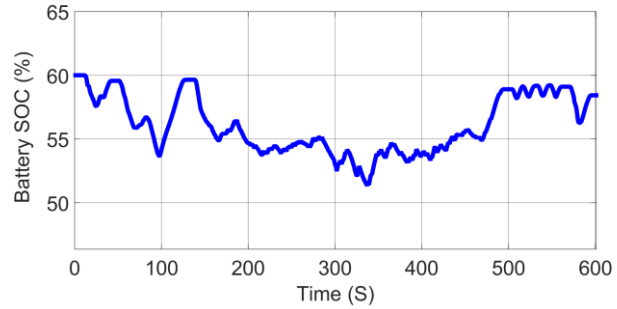


(d) Battery state of charge profile

Figure 12: RPEC controller simulation results for US06 driving cycle

Unlike the US06 and LA92 driving cycles, which are representative of an American aggressive highway and urban driving scenarios respectively, the ARTEMIS U130 driving cycle (Figure 14a) has been introduced in this study to assess the hybridisation potentials of the controller over an aggressive urban driving scenario in Europe. Similar to the LA92 driving cycle, frequent electric motor vehicle braking is observed over the ARTEMIS U130 driving cycle. Consequently, a near-charge-sustaining balance in energy of 59.28% (Figure 14d) is achieved with a cumulative fuel savings of 9.18% (Figure 14c).

The WLTC 3 driving cycle (Figure 15a) represents a moderate urban driving scenario in Europe. Unlike all other considered driving cycles in this section, the WLTC 3 driving cycle offers the opportunity to investigate the potency of the controller over a cycle which is representative of the most common urban driving scenario in Europe. The WLTC 3 driving cycleis characterised by numerous braking opportunities, which makes it possible for the controller to achieve a cumulative fuel savings of 13.73% (Figure 15d), with a final battery state of charge of 63.63%.

By combining the 11 driving cycles employed in this study (Table 4), a new driving profile that is 8647s (2.4 hours) long, as shown in Figure 16a, was developed to test the efficacy of the controller under a long (> 2 hours) and dynamically varying driving profiles such as a journey involving neighborhood, urban and highway driving at different aggressivity levels.

Owing to the high frequency of braking events which characterises this driving profile, a near-charge-sustaining performance of 59.82% (Figure 16d) with a cumulative fuel savings of 11.70% (Figure 16c) was achieved.

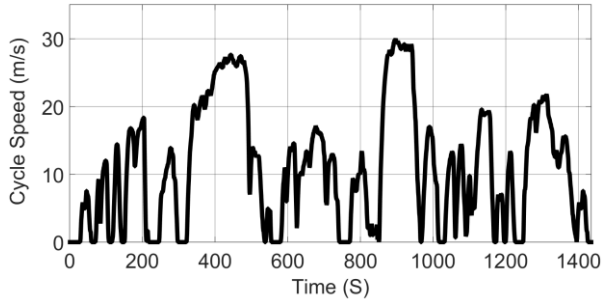


(a) LA92 driving cycle profile

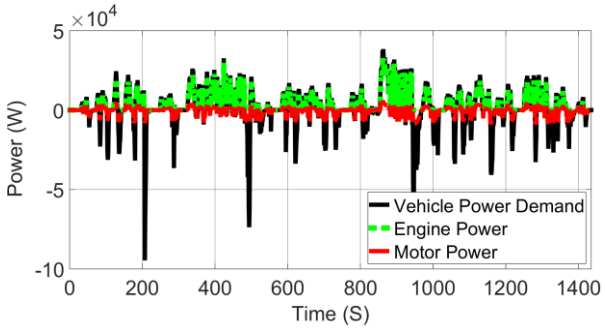


(b) Power split between electric motor and engine

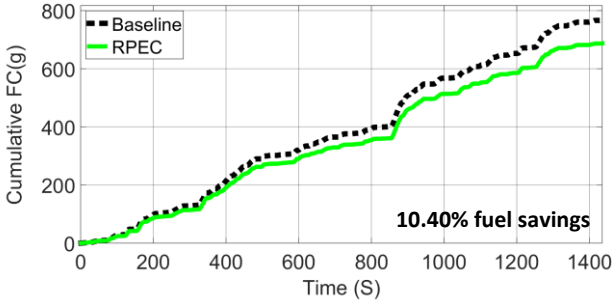


(c) Cumulative fuel consumption profile

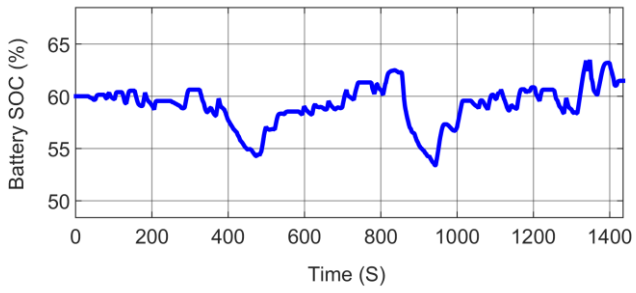


(d) Battery state of charge profile

Figure 13: RPEC controller simulation results for LA92 driving cycle

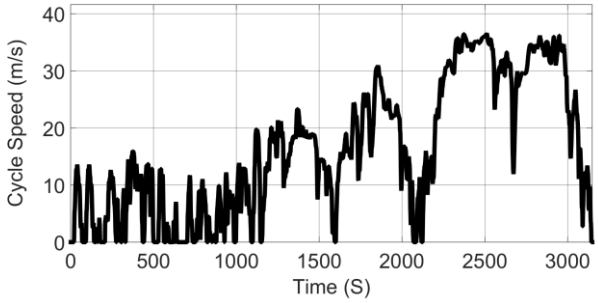


(a) ARTEMIS U130 driving cycle profile

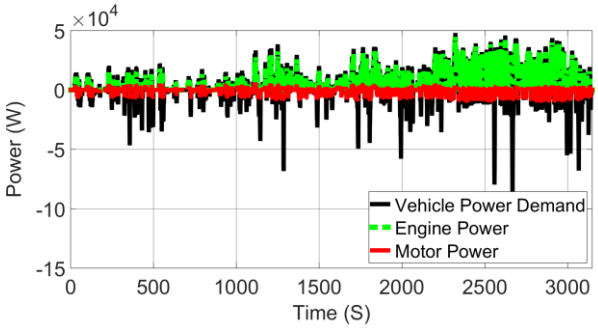


(b) Power split between electric motor and engine

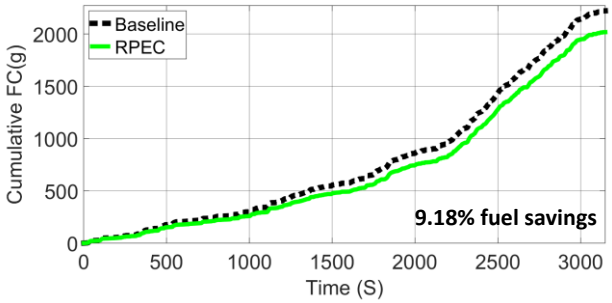


(c) Cumulative fuel consumption profile

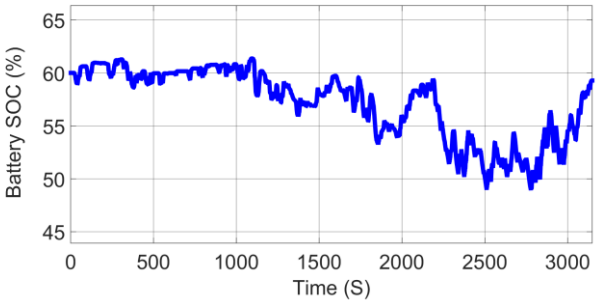


(d) Battery state of charge profile

Figure 14: RPEC controller simulation results for ARTEMIS U130 driving cycle

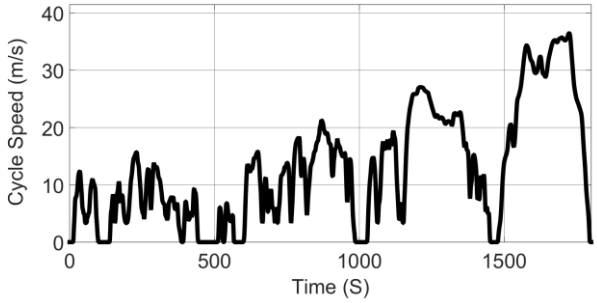


(a) WLTC 3 driving cycle profile

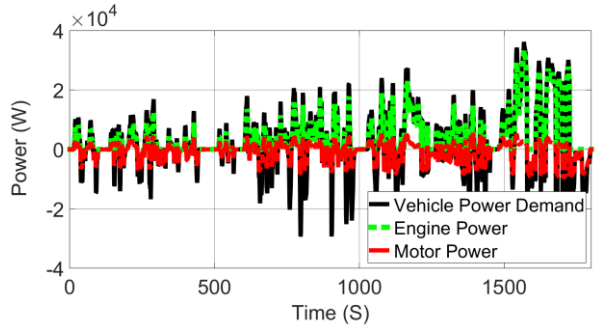


(b) Power split between electric motor and engine

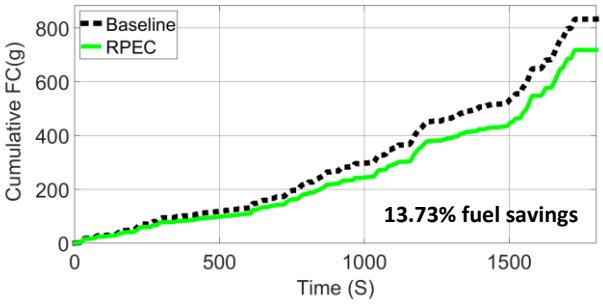


(c) Cumulative fuel consumption profile

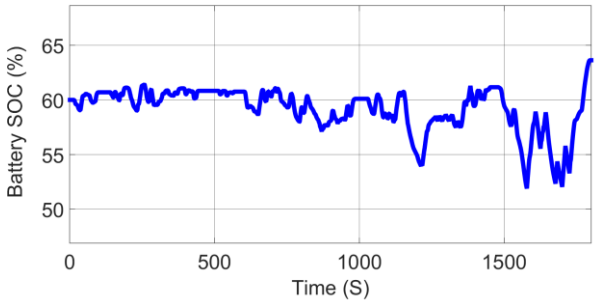


(d) Battery state of charge profile

Figure 15: REPC controller simulation results for WLTC 3 driving cycle

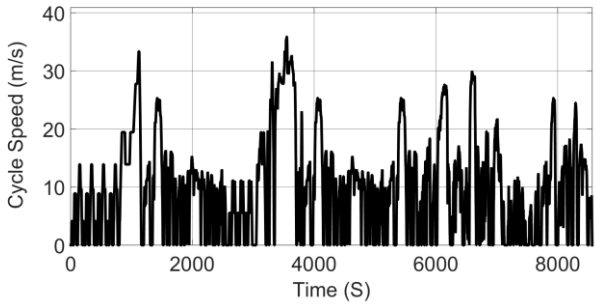


(a) Combination of 11 driving cycles

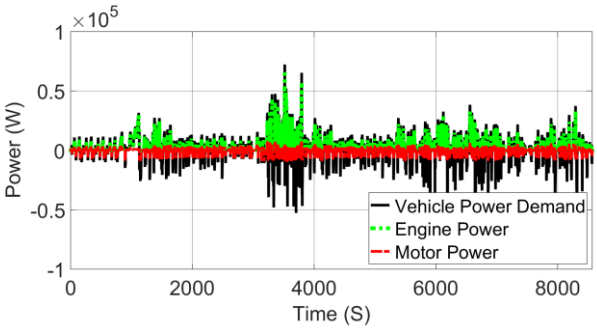


(b) Power split between electric motor and engine

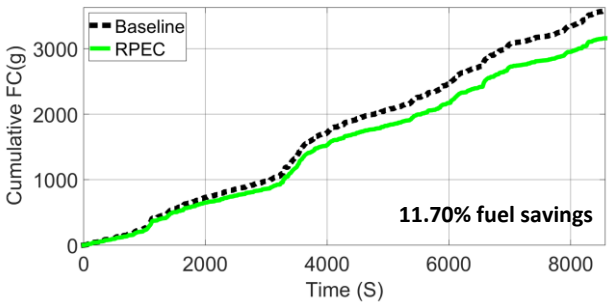


(c) Cumulative fuel consumption profile

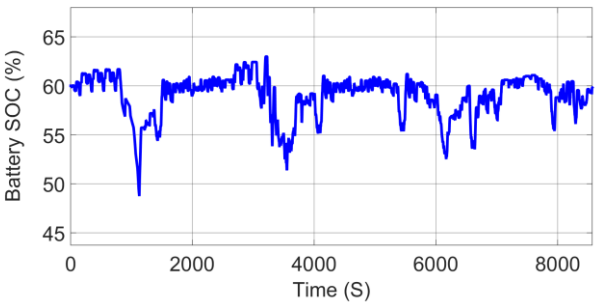


(d) Battery state of charge profile

Figure 16: RPEC controller simulation results for 11 combined driving cycles

### 5.4.2 Evaluation over real-world driving profiles

In this section, the hybridisation potentials of the RPEC controller are accessed in simulation over various real-world driving profiles, representing highway driving (Figure 17a), neighbourhood driving (Figure 18a) and urban driving (Figure 19a). The driving profiles used for this road test validation were obtained from a blind trial eco-drive study previously performed by *Vagg et al.* [46, 47] at the University of Bath, UK.

Over the highway driving profile (Figure 17a), 12.62% fuel savings was achieved with a near-charge-sustaining battery SOC of 59.14%. Over the neighbourhood driving profile (Figure 18a), much higher fuel savings (18.34%) were achieved with a near-charge-sustaining performance (61.06%) similar to that of the highway driving profile. During the road test, a peak value of 19.68% fuel savings was achieved over the urban driving profile (Figure 19a) with a near-charge-sustaining SOC of 60.23%.

Summarily, besides the US06 driving cycle which offers minimal braking events, the RPEC controller is able to guarantee, even on longer cycles and real-world driving profiles, promising fuel saving potentials, whilst effectively enforcing final battery state of charge deviations of less than 2%. It is, however, important to compare these results to those of similar existing SOC feedback ECMS controllers, with a view to highlighting the relative benefits. This comparison will be discussed in the next section.

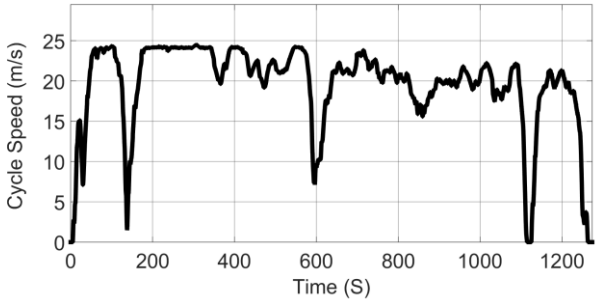


(a) Real world highway driving profile

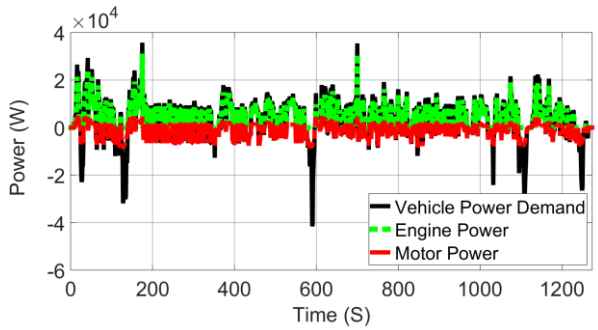


(b) Power split between electric motor and engine

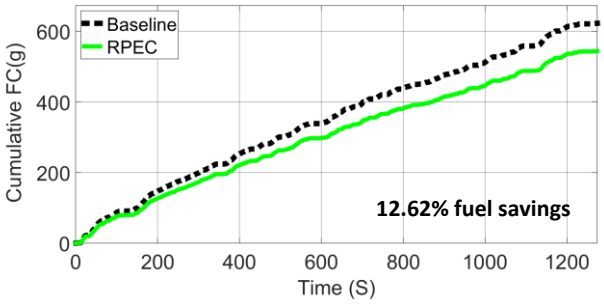


(c) Cumulative fuel consumption profile

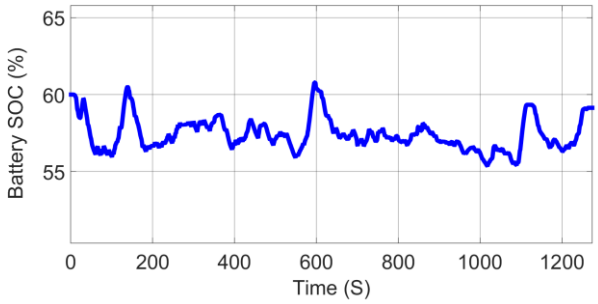


(d) Battery state of charge profile

Figure 17: RPEC controller simulation results for real world highway driving profile

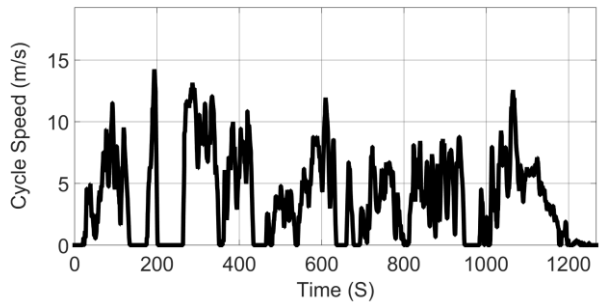


(a) Real world neighbourhood driving profile

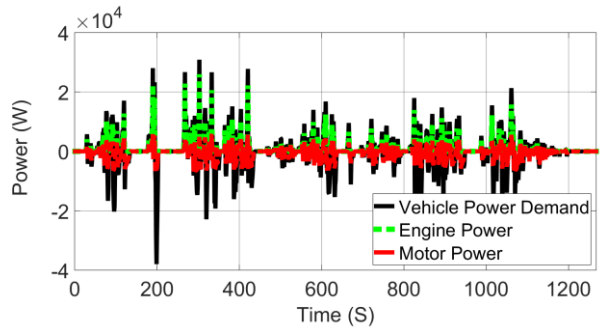


(b) Power split between electric motor and engine

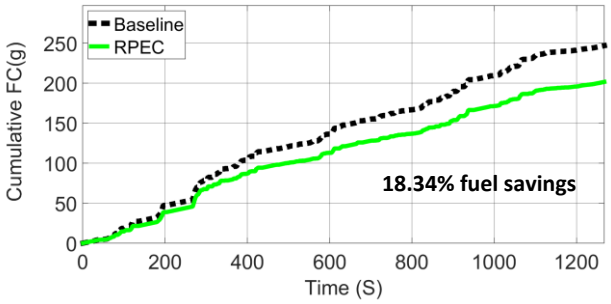


(c) Cumulative fuel consumption profile

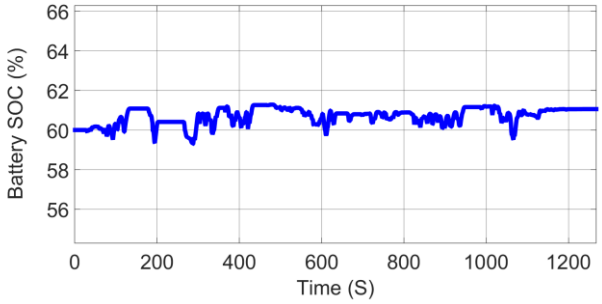


(d) Battery state of charge profile

Figure 18: RPEC controller simulation results for real world neighbourhood driving profile

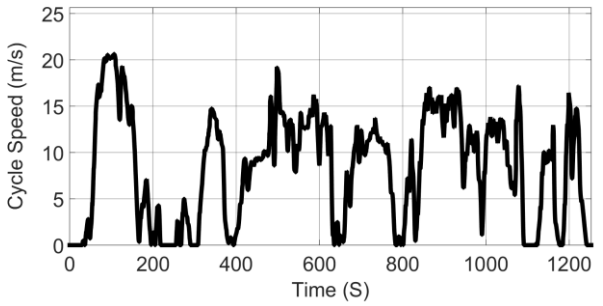


(a) Real world urban driving profile

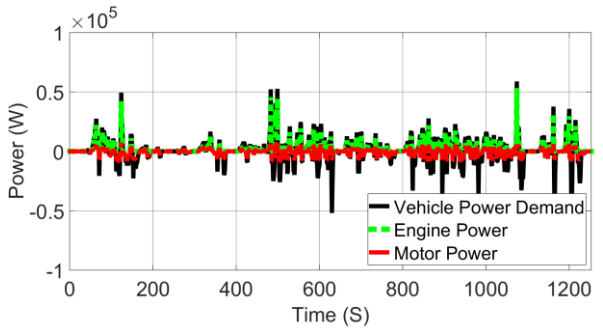


(b) Power split between electric motor and engine

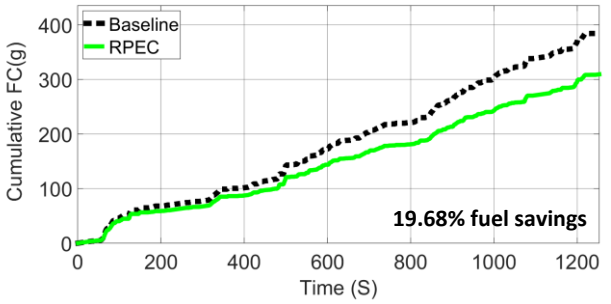


(c) Cumulative fuel consumption profile

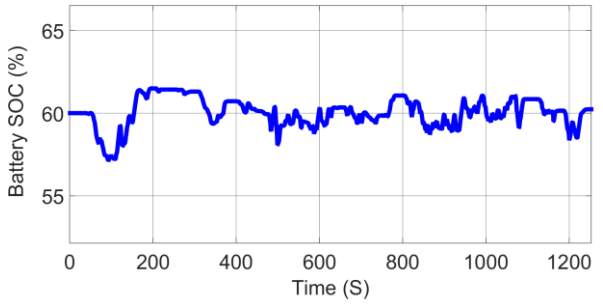


(d) Battery state of charge profile

Figure 19: RPEC controller simulation results for real world urban driving profile

A summary of the fuel-saving potentials derived from applying the RPEC controller to different driving profiles are detailed in Table 7.

| Driving cycle | Equivalence Factor | Proportional Controller gain | Cumulative Fuel Savings (%) | Final battery SOC (%) |
|---|---|---|---|---|
| US06 | 3.470 | 1.725 | 8.40 | 58.43 |
| LA92 | | | 10.40 | 60.61 |
| ARTEMIS U130 | | | 9.18 | 59.28 |
| WLTC 3 | | | 13.73 | 63.63 |
| Combination of 11 driving cycles | | | 11.70 | 59.82 |
| Highway real world driving profile | | | 12.62 | 59.14 |
| Neighbourhood real world driving profile | | | 18.34 | 61.06 |
| Urban real world driving profile | | | 19.68 | 60.23 |

Table 7: RPEC controller simulation results with an initial equivalence factor of 3.470 and a proportional controller gain 1.725

## 5.5 Comparison of the proposed controller against existing SOC feedback ECMS controllers

In this section, the RPEC controller is compared to existing SOC feedback controllers with different adaptation techniques over the US06, LA92 and ARTEMIS U130 driving cycles. Before carrying out this comparative analysis, it is imperative that we introduce the existing SOC feedback controllers in question.

One such controller is the "Static prediction (SP) based on SOC" controller[38], which is mathematically represented as follows.

When $SOC_t < SOC_{ref}$ 14

$$\varepsilon_t = \varepsilon_0\left(1 + \left(\frac{\tan\left(SOC_{ref} - SOC_t\right)\frac{\pi}{180}}{\tan\left(SOC_{ref} - SOC_{min}\right)\frac{\pi}{180}}\right)^n\right)$$

When $SOC_t > SOC_{ref}$

$$\varepsilon_t = \varepsilon_0\left(1 + \left(\frac{\tan\left(SOC_{ref} - SOC_t\right)\frac{\pi}{180}}{\tan\left(SOC_{ref} - SOC_{max}\right)\frac{\pi}{180}}\right)^n\right)$$

*n = 2,* $SOC_{ref} = 60\%$ , $SOC_{min} = 40\%$ ,$SOC_{max} = 80\%$

The second controller being considered is the "Adaptive prediction (AP) based on SOC" controller[38], which is mathematically represented as follows.

When $SOC_t < SOC_{ref}$ 15

$$\varepsilon_t = \varepsilon_{t-1}\left(1 + \left(\frac{\tan\left(SOC_{ref} - SOC_t\right)\frac{\pi}{180}}{\tan\left(SOC_{ref} - SOC_{min}\right)\frac{\pi}{180}}\right)^n\right)$$

When $SOC_t > SOC_{ref}$

$$\varepsilon_t = \varepsilon_{t-1}\left(1 + \left(\frac{\tan\left(SOC_{ref} - SOC_t\right)\frac{\pi}{180}}{\tan\left(SOC_{ref} - SOC_{max}\right)\frac{\pi}{180}}\right)^n\right)$$

$0 < \varepsilon_t < 40$ (Used to avoid integral build up), n = 2, $SOC_{ref} = 60\%$ , $SOC_{min} = 40\%$ , $SOC_{max} = 80\%$

Both AP and SP controllers employ the use of a tangent penalty function to regulate the battery SOC whenever it deviates from the reference SOC, which is 60%. In both controllers, whenever the battery SOC is close to the reference value, the penalty is negligible; however, the penalty function changes non-linearly as the SOC deviates from the reference value. The exponential coefficient governing the shape of the penalty function is n = 2.

Converse to the SP controller, the AP controller introduces some adaptability into the system, such that the initial equivalence factor has a negligible effect on the system performance. This adaptability is facilitated using the feedback of previous equivalence factors,

such that the centre of the tangent function is made to change according to trending values of the equivalence factor. In order to avoid an integral build-up in the system, the equivalence factor feedback for the "AP" controller is saturated at 40.

Over all the driving profiles analysed (Figures 20 to 22), the SP controller performance is found to be greatly affected by the initial equivalence factor ((Figure 20(a), Figure 21(a) and Figure 22(a)), which weakens the robustness of the controller, thus making it the least effective of all compared controllers.

In comparison to the RPEC controller, the AP controller is found to be inefficient over the US06 (Figure 20), LA92 (Figure 21) and ARTEMIS U130 (Figure 22) driving cycles. Over these driving cycles, both controllers deplete similar levels of battery energy, but the RPEC controller achieves higher fuel savings as shown in Figure 20a, Figure 21a, Figure 22a, for the US06, LA92 and ARTEMIS U130 driving cycles respectively.

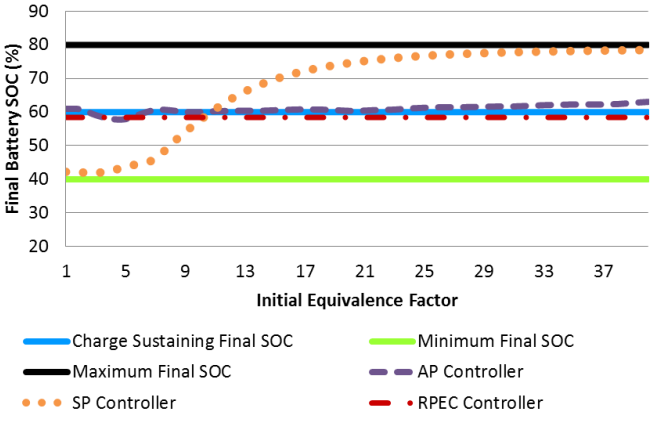


(a) Impact of initial equivalence factor on final battery state of charge

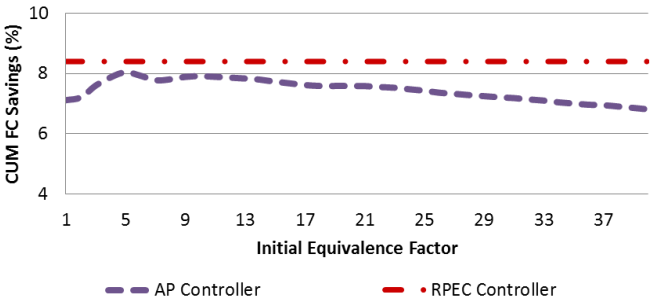


(b) Impact of initial equivalence factor on cumulative fuel savings

Figure 20: Comparison of SP, AP and RPEC controllers over the US06 driving cycle

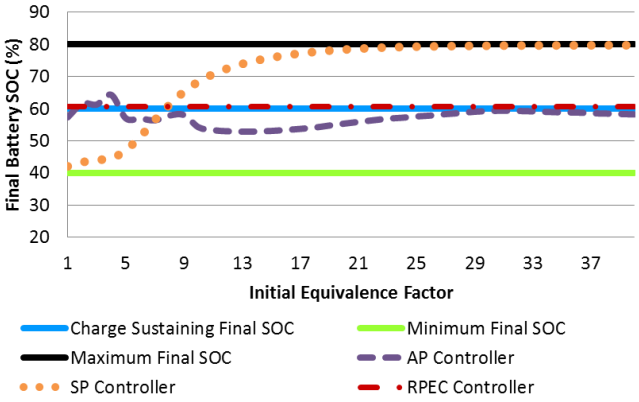


(a) Impact of initial equivalence factor on final battery state of charge

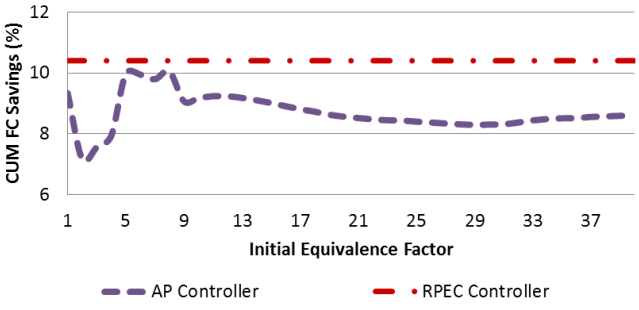


(b) Impact of initial equivalence factor on cumulative fuel savings

Figure 21: Comparison of SP, AP and RPEC controllers over the LA92 driving cycle

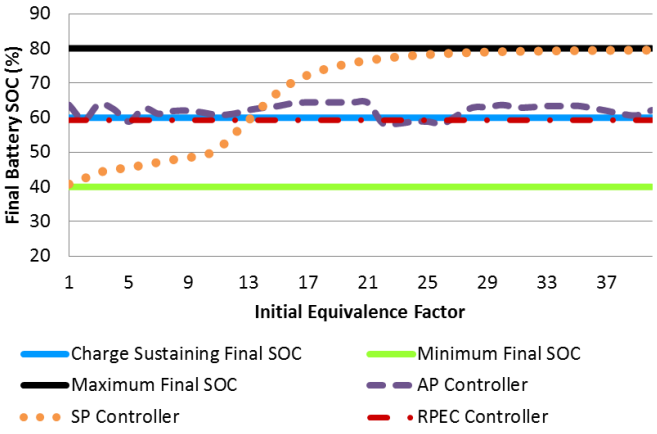


(a) Impact of initial equivalence factor on final battery state of charge

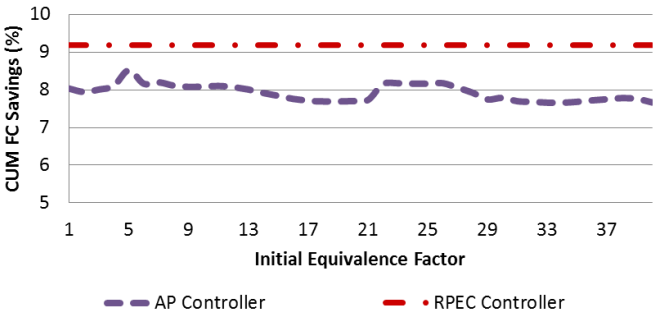


(b) Impact of initial equivalence factor on cumulative fuel savings

Figure 22: Comparison of SP, AP and RPEC controllers over the ARTEMIS U130 driving cycle

Based on the foregoing comparative analysis, the following general inferences could be drawn:

1. The SP controller performance is greatly affected by the intuitive estimate of the initial equivalence factor, which means that the controller can only provide promising and charge sustaining results if an accurate estimate of the initial equivalence factor is made. This shortcoming limits the usefulness of the SP controller and thus its viability for real-time implementation.

2. The AP controller introduces some adaptability into the control system by changing the centre of the tangent function in accordance to the trending values of the equivalence factor. By so doing, the AP controller is able to achieve a higher level of

charge sustenance when compared to the SP controller. That notwithstanding, the AP controller suffers from efficiency issues in that over the US06, LA92 and ARTEMIS U130 driving cycles, it is found to deplete similar battery energy levels as the RPEC controller but achieve less fuel savings.

3. The RPEC controller performs consistently well across all cycles examined, minimising the final SOC error compared to the other controllers examined. Its robustness and simultaneous optimisation of adaptation factors for charge sustenance and fuel reduction make it a promising option for real time implementation in commercial HEVs.

Simulation results of the RPEC controller over different driving scenarios are summarised in Table 8. This table compliments Table 7 with the addition of estimations for the fuel lost or gained due to non-charge sustenance. To make these estimations, Equation 16 is proposed and applied to this study.

$$FC_{savings\ deviation}(g) = \left(\left(\frac{SOC_{ref}}{2SOC_{ref} - SOC_{final}}\right)^{n} - 1\right) FC_{savings}(g) \quad (16)$$

Where:-

| | |
|---|---|
| $FC_{savings\ deviation}(g)$ is | Mass of fuel lost or gained due to non-charge sustenance |
| $FC_{savings}(g)$ is | Mass of fuel savings achieved by the RPEC controller |
| $SOC_{ref}$ | Charge-sustaining battery state of charge = 60% |
| $SOC_{final}$ | Final battery state of charge |

**Where:**

$n_c = 1$ *for charge hoarding controllers*
$n_c = 3$ *for charge depleting controllers*

$n_c = 3$ *is used in charge depleting controllers to account for the charge loses and thus the fuel consumption penalties associated with battery recharge due to unproductive reactions.*

These estimations are important as they provide an insight into the control penalties associated with using the RPEC controller over different driving scenarios.

| Driving Cycles | Cumulative fuel savings (g) | Cumulative fuel Savings (%) | Battery state of charge deviation (%) | Fuel lost or gained due to non charge sustenance (g) |
|---|---|---|---|---|
| **US06** | 50.92 | 8.40 | -1.57 | 4.41 |
| **LA92** | 79.81 | 10.40 | 0.61 | -0.82 |
| **ARTEMIS U130** | 204.03 | 9.18 | -0.72 | 8.33 |
| **WLTC 3** | 55.25 | 13.73 | 3.63 | -3.56 |
| **Combination of 11 driving cycles** | 418.36 | 11.70 | -0.18 | 4.35 |
| **Highway real world driving profile** | 78.62 | 12.62 | -0.86 | 3.83 |
| **Neighbourhood real world driving profile** | 45.29 | 18.34 | 1.06 | -0.81 |
| **Urban real world driving profile** | 75.81 | 19.68 | 0.23 | -0.29 |

Table 8: RPEC controller simulation results summary

Fuel gained: (+), Fuel lost: (-)

## 6 CONCLUSIONS AND FURTHER WORK

This paper offers a detailed insight into ECMS optimal control. First, a theoretical framework for ECMS control is developed from the PMP. From this derivation, it is shown that, based on the assumption that the effect of the battery SOC on the equivalence factor is negligible; the equivalence factor could be considered as a constant parameter, thus reducing the complexity of the optimal control problem. Physically, the equivalence factor represents the equivalent conversion ratio between the thermal energy from fuel and electrical energy. Using a one-dimensional sensitivity analysis, a low equivalence factor was shown to imply that electrical energy is cheaper than fuel; therefore, the controller encourages battery use, while a high equivalence factor implies that using electrical energy is expensive. Therefore, the controller reduces battery use.

Analysis on the impact of the equivalence factor on the fuel saving potentials of the modelled vehicle was undertaken over different driving cycles. The following useful inferences were drawn from this analysis: (1) A single but cycle-specific optimal equivalence factor is responsible for charge sustenance (final battery SOC = 60%) over each driving cycle. (2) A slight deviation in the estimation of the optimal equivalence factor would yield an undesired controller performance, which is non-charge sustaining in real time. (3)The equivalence factor is found to correlate inversely with cumulative fuel savings and proportionately with final battery state of charge.

Based on observations from the foregoing or aforementioned analysis, problems impeding the commercial implementation of ECMS optimal control were identified alongside some key solutions that have been proposed in literature. Despite the proposed solutions, the problem of non-robustness (non-adaptability to varying driving conditions) for ECMS controllers still remained unaddressed and, as such, was considered the main inspiration for this study.

In order to address the non-robustness issue currently associated with ECMS controllers, a proportional ECMS control strategy was proposed. This strategy works by adapting equivalence factors based on battery state of charge feedback. The proposed adaptation strategy differs conceptually from existing SOC feedback adaptation strategies in that the method simultaneously optimises and selects the adaptation factors (proportional controller gain and initial equivalence factor) as single parameters which can be applied in real-time over any driving cycle. Unlike other existing SOC feedback methods, this approach solves a conflicting multi-objective optimisation control problem, thus ensuring that the obtained adaptation factors are optimised for robustness, charge sustenance and fuel reduction.

Using a two dimensional sensitivity analysis, the appropriate adaption factors for application in real-time were selected (initial equivalence factor = 3.47 and proportional controller gain = 1.725) and applied over a range of driving profiles. Hybridisation fuel saving potentials of approximately 8.40%, 10.40%, 9.18% and 13.73% were observed over the US06, LA92, ARTEMIS U130 and WLTC 3 driving cycles respectively. A similar analysis undertaken was over three real-world driving profiles, representing: highway, neighbourhood and urban driving. Over these driving profiles, the following near-charge-sustaining fuel-saving performances were achieved: highway driving (12.62% fuel savings, 59.14% final battery state of charge), neighbourhood driving (18.34% fuel savings, 61.06% end battery state of charge), and urban driving (19.68% fuel savings, 60.23% final battery state of charge).

In comparison to existing SOC feedback ECMS controllers, the RPEC controller was found to perform well, specifically in two key areas. The first being that the controller appears robust and unaffected by the intuitive estimate of the initial equivalence factor as in the case of the “SP controller” and the second being that the controller is highly efficient. Over the US06, LA92 and ARTEMIS U130 driving cycles, it was shown that the “AP controller“ in comparison to the RPEC controller, depleted similar levels of battery energy but achieved less fuel savings.

Despite the significant fuel savings predicted in this study, the absence of route preview information from the proposed control framework means that route

elevation changes are not accounted for during the equivalence factor adapation, thus limiting the robustness of the RPECcontroller to flat terrains only. Future reasearch studies should aim to incorportate route elevation information (in the form of "route-optimised SOC trajectory") into thecontrol framework. Although the inclusion of this route elevation information may or may not directly translate to further fuel savings, the evisaged extra robustness to be gained makes it a worthwhile pursuit. Experimental validation of the fuel savings reported in this paper will also form a major part of future research.


## ACKNOWLEDGEMENT

The authors would like to thank Ashwoods Automotive for providing us with the engine experimental test data used for this research.


## NOMENCLATURE

### General Nomenclature

| | |
|---|---|
| AGF | Aggressivity Factor |
| NEDC | New European Driving Cycle |
| FTP | Federal Test Procedure |
| WLTC | Worldwide Harmonized Light duty Driving Test Cycle |
| US | United States |
| NYCC | New York City Cycle |
| IM | Inspection and Maintenance |
| SC | Supplementary Driving Cycle |
| LA | Los Angeles |
| ARTEMIS | Assessment and Reliability of Transport Emission Models and Inventory Systems |
| HWFET | Highway Fuel Economy Test |
| ECMS | Equivalent Consumption Minimisation Strategy |
| HEV | Hybrid Electric Vehicle |
| FC | Fuel Consumption |
| CUM | Cumulative |
| RPEC | Robust Proportional ECMS Control |
| ICE | Internal Combustion Engine |
| AP | Adaptive Prediction |
| SP | Static Prediction |
| SOC | State of charge |

### Vehicle Dynamics and Engine

| | |
|---|---|
| $F_{grade}$ | Resistance force by grade (N) |
| $F_{extra}$ | Extra tractive force needed for the vehicle to achieve the requested vehicle speed (N) |
| $F_{aero}$ | Aerodynamic drag force (N) |
| $F_{rolling}$ | Rolling resistance force (N) |
| $Eff$ | Drive train efficiency |
| FDR | Final drive ratio |
| $G_E$ | Engine gear ratio |
| $G_M$ | Motor gear ratio |
| $T_{ICE}$ | Tractive torque from internal combustion engine (Nm) |
| $W_{ICE}$ | Engine speed (RPM) |
| $W_{wheel}$ | Wheel Speed (RPM) |
| $R_w$ | Radius of rolling wheels (m) |

### Electrical Motor

| | |
|---|---|
| $P_{motor}$ | Motor mechanical power (W) |
| $\eta_{motor}$ | Motor efficiency |
| $P_{motor\,max}$ | Maximum motor tractive power (W) |
| $w_{motor}$ | Motor speed (RPM) |

### Electrical Battery

| | |
|---|---|
| $V_{oc}$ | Battery open circuit voltage (V) |
| $V_{batt}$ | Battery voltage (V) |
| $R$ | Battery resistance (Ohms) |
| $SOC_{t+1}$ | Future battery state of charge |
| $SOC_t$ | Present battery state of charge |
| $SOC_{min}$ | Minimum battery state of charge |
| $SOC_{max}$ | Maximum battery state of charge |
| $t$ | Present simulation time (s) |
| $t$+1 | Future simulation time (s) |
| $I_t$ | Battery current (A) |
| $Q$ | Battery capacity (Ah) |
| $\eta_{batt}$ | Overall battery efficiency |

| | |
|---|---|
| $\eta_{dis}$ | Battery discharge efficiency |
| $\eta_{chg}$ | Battery charge efficiency |
| $\eta_{gen}$ | Generator efficiency |

## RPEC controller

| | |
|---|---|
| $\varepsilon_t$ | Equivalence factor |
| $\varepsilon_0$ | Initial equivalence factor |
| $LHV$ | Lower heating value of fuel (J/Kg) |
| $\gamma_t$ | Controller costate |
| $\dot{m}_{f\ engine}$ | Engine fuel cost (g/s) |
| $\dot{m}_{f\ eq}$ | Equivalent fuel cost (g/s) |
| $SOC_{ref}$ | Charge sustaining SOC |
| $K_{ps}$ | Proportional controller gain |

## REFERENCES


[1] Brahma A, Guezennec Y, Rizzoni G. Dynamic Optimization of Mechanical/Electrical Power Flow in Parallel Hybrid Electric Vehicles. in: Proceedings of 5th Int Symposium in Advanced Vehicle Control, Ann Arbor, MI. 2000.

[2] Schouten NJ, Salman MA, Kheir NA. Energy Management Strategies for Parallel Hybrid Vehicles Using Fuzzy Logic. Control Engineering Practice. 2003;vol. 11:171-7.

[3] Delprat S, Lauber J, Guerra TM. Control of a Parallel Hybrid Powertrain: Optimal Control. IEEE Transactions on Vehicular Technology. 2004;vol. 53:872-81.

[4] Takaishi T, Numata A, Nakano R, Sakaguchi K. Approach to High Efficiency Diesel and Gas Engines. Mitsubishi Heavy Industries, Ltd Technical Review. 2008;vol. 45.

[5] Leduc P, Dubar B. Downsizing of Gasoline Engine: An Efficient Way to Reduce CO2 Emissions. Oil & Gas Science and Technology. 2003;vol. 58:115–27.

[6] Mercier C. Advanced Powertrain Controls. Lecture at IFP School PSA Peugeot Citroën. 2012.

[7] Chen J, Li Y, Wang J. Simultaneous Optimisation of Fuel Consumption And Emissions For a Parallel Hybrid Electric SUV Using Fuzzy Logic Control. International journal of vehicle design. 2008;vol. 46:204–18.

[8] Schouten NJ, Salman MA, Kheir NA. "Fuzzy logic control for parallel hybrid vehicles". IEEE Transaction on Control Systems Technology. 2002;vol. 10, 460.

[9] Guzzella L, Sciarretta A. "Vehicle Propulsion Systems". Springer; 2005.

[10] Baumann BM, Washington G, Glenn BC, Rizzoni G. "Mechatronic design and control of hybrid electric vehicles". IEEE/ASME Trans Mechatronics. 2000;vol. 5:pp. 58–72.

[11] Powell BK, Bailey KE, Cikanek SR. "Dynamic modeling and control of hybrid electric vehicle powertrain systems". IEEE Control Syst Mag. 1998;vol. 18:pp. 17–33.

[12] Rizoulis D, Burl J, Beard J. Control Strategies for a Series-Parallel Hybrid Electric Vehicle. SAE, Warrendale, PA. 2001;Paper No. 2001-01-1354.

[13] Sharer PB, Rousseau A, Karbowski D, Pagerit S. Plug-in Hybrid Electric Vehicle Control Strategy: Comparison Between EV and Charge-Depleting Options. SAE, Warrendale, PA. 2008;Paper No. 2008-01-0460.

[14] Rousseau A, Pagerit S, Gao D. "Plug-in hybrid electric vehicle control strategy parameter optimization". Electric Veh Symp-23, Anaheim, CA2007.

[15] Sciarretta A, Guzzella L. Rule-Based and Optimal Control Strategies for Energy Management in Parallel Hybrid Vehicles. 6th International Conference on Engines for Automobile (ICE 2003). 2003.

[16] Opila DF, Wang X, McGee R, Cook A, Grizzle JW. Fundamental Structural Limitations of an Industrial Energy Management Controller Architecture for Hybrid Vehicles. ASME Dynamic Systems and Control Conference. 2009.

[17] Brahma A, Guezennec Y, Rizzoni G. "Optimal energy management in series hybrid electric vehicles". Proceedings of the American Control Conference. 2000.

[18] Back M, Simons M, Kirschaum F, Krebs V. Predictive Control of Drivetrains. in: Proceedings of IFAC 15th Triennial World Congress, Barcelona, Spain. 2002;vol. 35:241–6.

[19] Lin C-C, Peng H, Grizzle JW, Kang J-M. "Power management strategy for a parallel hybrid electric truck". IEEE Trans Contr Syst Technol. 2003;vol. 11, no. 6:pp. 839–49.

[20] Arsie I, Graziosi M, Pianese C, Rizzo G, Sorrentino M. "Optimization of supervisory control strategy for parallel hybrid vehicle with provisional load estimate". Proc 7th Int Symp Adv Vehicle Control (AVEC), Arnhem, The Netherlands. 2004.

[21] Lin C, Kang J, Grizzle JW, Peng H. "Energy Management Strategy for a Parallel Hybrid Electric Truck". Proceedings of the 2001 American Control Conference, Arlington, VA. 2001:pp.2878-83.

[22] O'Keefe MP, Markel T. "Dynamic programming applied to investigate energy management strategies for a plug-in HEV". National Renewable Energy Laboratory, Golden, CO. 2006;Report No. NREL/CP-540-40376.

[23] Gong Q, Li Y, Peng Z-R. "Trip-based optimal power management of plug-in hybrid electric vehicles". IEEE Trans Veh Technol. 2008;vol. 57, no. 11:pp. 3393–401.

[24] Kum D, Peng H, Bucknor NK. Supervisory Control of Parallel Hybrid Electric Vehicles for Fuel and Emission Reduction. Journal of Dynamic Systems, Measurement, and Control. 2011;vol. 133.

[25] Paganelli G, Delprat S, Guerra TM, Rimaux J, Santin JJ. "Equivalent consumption minimization strategy for parallel hybrid powertrains". Proc IEEE 55th Vehicular Technology Conference. 2002;volume 4:pages 2076–81.

[26] Pisu P, Rizzoni G. A Comparative Study of Supervisory Control Strategies for Hybrid Electric Vehicles. IEEE Trans on Control SystemsTechnology. 2007;vol. 15:506–18.

[27] Kleimaier A, Schr¨oder D. An Approach for the Online Optimized Control of a Hybrid Powertrain. in: Proceedings of 7th International Workshop Advanced on Motion Control. 2002:215–20.

[28] Rizzoni G, Pisu P, Calo E. Control Strategies for Parallel Hybrid Electric Vehicles. in: Proceedings of IFAC Symposium on Advanced Automotive Control. 2004:508–13.

[29] Sciarretta A, Back M, Guzzella L. Optimal Control of Parallel Hybrid Electric Vehicles. IEEE Transactions On Control Systems Technology. 2004;vol. 12.

[30] Delprat S, Guerra TM, Rimaux J. "Optimal Control of a Parallel Powertain: From Global Optimization to Real Time Control Strategy". Proc of the 18th Electric Vehicle Symposium, EVS18. 2001.

[31] Kim N, Cha S, Peng H. "Optimal Control of Hybrid Electric Vehicles Based on Pontryagin's Minimum Principle". IEEE TRANSACTIONS ON CONTROL SYSTEMS TECHNOLOGY. 2011;VOL. 19, NO. 5.

[32] Kim N, Cha S, Peng H. "Optimal Control of Hybrid Electric Vehicles Based on Pontryagin's Minimum Principle". IEEE Trans Contr Syst Technol. 2011;19(5):pp.1279-87.

[33] Serrao L, Onori S, Rizzoni G. ECMS as a Realization of Pontryagin's Minimum Principle for HEV Control. in: American Control Conference, IEEE. 2009:3964-9.

[34] Musardo C, Rizzo G, Staccia B. "A-ECMS: An adaptive algorithm for hybrid electric vehicle energy management". In Proc Decision and Control Conference and European Control Conference. 2005:pages 1816–23.

[35] Onori S, L S, Rizzo G. "Adaptive equivalent consumption minimization strategy for HEVs". In 3rd Annual Dynamic Systems and Control Conference, Cambridge, MA. 2010.

[36] Cente for Advanced Automotive Technology. HEV Levels. http://autocaatorg/Technologies/Hybrid_and_Battery_Electric_Vehicles/HEV_Levels/). 22 May 2016.

[37] Sciarretta A, Guzzella L, Back M. "A real-time optimal control strategy for parallel hybrid vehicles with on-board estimation of control parameters". Proc IFAC Symposium on Advances Automotive Control, Salerno, Italy. 2004:pages 502–7.

[38] Sivertsson M, Sundstrom C, Eriksson L. Adaptive Control of a Hybrid Powertrain with Map-based ECMS. IFAC World Congress. 2011.

[39] Enang W, Bannister C, Brace C, Vagg C. Modelling and Heuristic Control of a Parallel Hybrid Electric Vehicle. in: Proceedings of the Institution of Mechanical Engineers, Part D: Journal of Automobile Engineering 2015.

[40] Pontryagin L, Boltyanskii V, Gamkrelidze R, E. M. Mathematical Theory Of Optimal Processes. New York: Interscience Publishers. 1962.

[41] Barlow T, Latham S, McCrae I. A Reference Book of Driving Cycles For Use In The Measurement of Road Vehicles Emissions. Published Project Report 354 Department for Transport, Clearner Fuels & Vehicles Transport Research Laboratory. 2009;version 3:284.

[42] Berry I. "The Effect of Driving Style and Vehicle Performance on the Real-World Fuel Consumption of U.S. Light-Duty Vehicles". Massachusetts Institute of Technology2010.

[43] Won J, Langari R, Ehsani M. "An energy management and charge sustaining strategy for a parallel hybrid vehicle with CVT". Control Systems Technology , IEEE Transactions 2005. p. pp. 313–20.

[44] Jeon S, Jo S, Park Y, Lee J. Multi-Mode Driving Control of a Parallel Hybrid Electric Vehicle Using Driving Pattern Recognition. ASME Journal of dynamic systems, measurement, and control. 2002;vol. 124:141–9.

[45] Koot M, Kessels A, Jager B, Heemels W, Bosch P, Steinbuch M. Energy Management Strategies for Vehicular Electric Power Systems. IEEE Transactions on Vehicular Technology. 2005;vol. 54:771–82.

[46] Vagg C, Brace C, Hari D, Akehurst S, Poxon J, Ash L. Development and Field Trial of a Driver Assistance System to Encourage Eco-Driving In Light Commercial Vehicle Fleets. IEEE Transactions on Intelligent Transportation Systems. 2013;vol. 14:796-805.

[47] Vagg C, Brace C, Hari D, Akehurst S. A Driver Advisory Tool to Reduce Fuel Consumption. SAE Technical Paper 2012-01-2087. 2013:6.

## APPENDICES

**Appendix 1**: Vehicle modelling data

| | | |
|---|---|---|
| **Vehicle Type** | Light Commercial | |
| **Fuel** | Diesel | |
| **Engine** | 1.6HDi 90hp | |
| **Transmission** | Gear 1 | 11/38 |
| | Gear 2 | 15/28 |
| | Gear 3 | 32/37 |
| | Gear 4 | 45/37 |
| | Gear 5 | 50/33 |

**Vehicle Parameters**

| | |
|---|---|
| Wheel Radius | 0.307 meters |
| Drag Coefficient | 0.35 |
| Rolling Resistance | 0.001 |
| Vehicle Mass | 1360 Kg |
| Final Drive Ratio | 4.2941 |
| Car Frontal Area | $2m^2$ |
| Drive Train Efficiency | 1 |
| Maximum Engine Speed | 6500 RPM |

**Battery Parameters**

| | |
|---|---|
| Battery Cell Composition | Lithium Ion Phosphate |
| Battery Capacity | 16 Ampere hours |
| Battery Resistance | 0.024 Ohms |
| Minimum State of Charge | 40% |
| Maximum State of Charge | 80% |
| Battery Open Circuit Voltage | 60V |

**Electric Motor Parameters**

| | |
|---|---|
| Motor Manufacturer | Perm Motor Germany |
| Motor Type | Brushless DC motor |
| Motor Model | PMS 120 |
| Max Motor Torque | 42 Nm |
| Max Motor Speed | 4500 RPM |
| Motor Gear Ratio | 1.178 |